Frequency-selected enhancement of high-order-harmonic generation by interference of degenerate Rydberg states in a few-cycle laser pulse

Jigen Chen,[1,2] Ruquang Wang,[2] Zhen Zhai,[2] Jing Chen,[3,4] Panming Fu,[2] Bingbing Wang,[2,*] and Wu-Ming Liu[2]

[1]*Department of Physics and Materials Engineering, Taizhou University, Taizhou 318000, China*

[2]*Beijing National Laboratory for Condensed Matter Physics, Institute of Physics, Chinese Academy of Sciences, Beijing 100190, China*

[3]*Key Laboratory of High Energy Density Physics Simulation, CAPT, Peking University, Beijing 100084, China*

[4]*Institute of Applied Physics and Computational Mathematics, P. O. Box 8009, Beijing 100088, China*

(Received 27 March 2012; published 17 September 2012)

We demonstrate that the frequency-selected enhancement of high-order-harmonic generation (HHG) can be achieved by a few-cycle laser pulse interacting with a coherent superposition state, which is prepared by the ground state and two degenerate Rydberg states. The degenerate states have the same orbital radius and hence have a large overlap in the electronic density distribution. By controlling the relative phase between the two degenerate states, the constructive or destructive interference of them can markedly change the initial density distribution of the Rydberg electron, thereby we can manipulate the characteristics and the conversion efficiency of HHG. Specifically, a significant enhancement in the continuous harmonics near HHG cutoff can be obtained, hence an intense isolated pulse with a duration less than 100 attoseconds is straightforwardly generated. On the other hand, since there exists a specific dependence of the harmonic efficiency on the relative phase of the two degenerate states, one can expect that the relative phase may be probed by examining the corresponding harmonic intensity. In practice, we may apply a weak static electric field in the whole dynamic process to obtain an asymmetry electron density distribution at a large radius; hence similar HHG results can be obtained.

DOI: 10.1103/PhysRevA.86.033417 PACS number(s): 32.80.Rm, 42.50.Hz, 32.80.Fb

I. INTRODUCTION

When intense lasers interact with atoms and molecules, high-order harmonic can be generated as a consequence of highly nonlinear dynamics [1–12]. The procedure of high-order-harmonic generation (HHG) can be described by the semiclassical recollision model [13] that consists of three steps: the tunnel ionization of a bound electron, the acceleration of the ionized electron in the laser field, and its recombination with the parent ion leading to the emission of high harmonics. HHG is a very useful source for generating coherent soft x-ray or extreme ultraviolet (XUV) light [14–17]. It has also been used for the production of isolated attosecond pulses or pulse trains, which opens up new opportunities for ultrafast time-resolved spectroscopy [18–22].

For both spectroscopic applications and the optimization of attosecond pulses, it is necessary to enhance a single harmonic or consecutive harmonics in a certain range. Bartels *et al.* [23] increased a particular harmonic order by carefully tailoring the shape of intense laser pulses with an evolutionary algorithm. Pfeifer *et al.* [24] demonstrated the enhancement and the suppression of several selected harmonics by the adaptive control of the driving laser pulse. They found that the manipulation of discrete harmonic peaks can modify the corresponding attosecond pulse trains. For some practical applications, an isolated attosecond pulse is preferable to a chain of attosecond pulses. Therefore, one may expect to enhance the conversion efficiency of the continuum part in the HHG cutoff region.

Recently, we studied HHG in an ultrashort laser pulse with the initial state being prepared as a coherent superposition of the ground state and a Rydberg state. It was found that the Rydberg electron with a large orbital radius can be accelerated directly toward the core under the influence of a few-cycle laser pulse, leading to the one-to-one correspondence relationship between the initial location of the electron and the harmonic order, and a broadband continuum spectrum around the HHG cutoff can be generated [25,26]. In this paper, we propose a method for selectively enhancing the continuous harmonics in the cutoff region by using the interference of two degenerate Rydberg states in a few-cycle pulse. Taking advantage of the large overlap of two degenerate states in the electronic density distribution, we show that the initial density distribution of the Rydberg electron can be changed effectively by controlling the relative phase of the two Rydberg states, resulting in the obvious change of the characteristics and brightness of HHG. In particular, our method can obviously increase the intensity of the broadband continuum harmonics near HHG cutoff, which produces directly an intense isolated 39-attosecond pulse with a bandwidth of 106 eV. Moreover, by adjusting the peak intensity of the few-cycle laser or adopting a pair of suitable degenerate states, the frequency-selected enhancement of the continuous HHG can be obtained in a wide frequency region, which may lead to an intense isolated attosecond pulse with a controlled central frequency.

II. THEORETICAL METHOD

We use the three-dimensional (3D) time-dependent Schrödinger equation (TDSE) to describe the interaction between a linearly polarized laser pulse and a single-active-electron atom model with the ionization potential of neon (atomic units are used throughout, unless otherwise stated)

$$i\frac{\partial}{\partial t}\psi(\mathbf{r},t)=\left[-\frac{1}{2}\nabla^2-\frac{Z_{\text{eff}}}{r}+\mathbf{E}(t)\cdot\mathbf{r}\right]\psi(\mathbf{r},t), \quad (1)$$

*wbb@aphy.iphy.ac.cn.

where the effective nuclear charge is chosen to be $Z_{\rm eff} = 1.2592$ to reproduce the same ionization threshold as the ground state of neon and the electric field $\mathbf{E}(t)$ of the laser pulse is along the z axis. The TDSE can be solved numerically in the spherical coordinate system by using the finite-difference technique [27]. Our integration grid is confined in a finite space $r < 800$ with the spatial step 0.1, and the time increment is 0.007. To avoid reflections of the wave function from the boundaries, the wave function after each time interval is multiplied by a $\cos^{1/8}$ mask function, which varies from 1 to 0 in the range of 750–800 [28].

The initial state is prepared in a coherent superposition of the ground state Ψ_{1s} and two degenerate Rydberg states Ψ_{ns} and Ψ_{np}

$$\Psi_{1s+ns+np}(\mathbf{r},t=0) = \sqrt{\frac{2}{5}}\Psi_{1s}e^{i\delta_0} + \sqrt{\frac{3}{10}}\Psi_{ns+np}, \qquad (2)$$

where

$$\Psi_{ns+np} = \Psi_{ns}e^{i\delta} + \Psi_{np}, \qquad (3)$$

n is the principal quantum number of the two Rydberg states, δ_0 is the phase difference between $1s$ and np, and δ is the relative phase of ns and np. We find that the results are insensitive to variations in δ_0, hence we set $\delta_0 = 0$ for simplicity throughout this paper. The amplitudes of the degenerate Rydberg states can be controlled by excitation of the atom in a suitable intense laser pulse, and the phase difference δ between the two degenerate states can be controlled by a dc electric field, which causes a Stark splitting of degenerate Rydberg states for a short time. Ryabtsev *et al.* [29] have demonstrated experimentally that such a process can be realized by using quantum interferometry of degenerate Rydberg states.

Degenerate states have the advantage of having the same orbital radius and hence have a large overlap in the electronic density distribution. For example, $6s$ and $6p$ atomic states have the same radius around 50 a.u. and greater amplitude near the radius region, as shown in Fig. 1. Therefore, the constructive or destructive interference of $6s$ and $6p$ may be achieved by controlling their relative phase δ. In the following, we consider three cases as $\delta = 0$, $\pi/2$, and π. The coherent superposition of $6s$ and $6p$ states is given by

$$\begin{aligned}\Psi_{6s+6p} &= \Psi_{6s}e^{i\delta} + \Psi_{6p} \\ &= \sqrt{\frac{1}{4\pi}}R_{6s}(r)e^{i\delta} + \sqrt{\frac{3}{4\pi}}R_{6p}(r)\cos\theta, \end{aligned} \qquad (4)$$

where θ is the angle between the radial direction and the $+z$ axis, R_{6s} (R_{6p}) is the radial component of the $6s$ ($6p$) wave function. In the case of $\delta = 0$, the superposition state is $\Psi_{6s+6p} = \Psi_{6s} + \Psi_{6p}$, thereby the electron probability is expressed as

$$|\Psi_{6s+6p}|^2 = |\Psi_{6s}|^2 + |\Psi_{6p}|^2 + \frac{\sqrt{3}}{2\pi}R_{6s}(r)R_{6p}(r)\cos\theta. \qquad (5)$$

As depicted in Fig. 1(c), R_{6s} and R_{6p} have almost the same magnitude but opposite sign. At the same time, $\cos\theta$ is positive (negative) in the regions $0^\circ < \theta < 90^\circ$ and $270^\circ < \theta < 360^\circ$ ($90^\circ < \theta < 270^\circ$). Therefore, there exists a destructive (constructive) interference between $6s$ and $6p$ in the $+z$ ($-z$) side, which results in an obvious decrease (enhancement) of the initial electronic density distribution, as shown in Fig. 2(a). On the contrary, for the case of $\delta = \pi$, the superposition state is $\Psi_{6s+6p} = \Psi_{6p} - \Psi_{6s}$, the corresponding electron probability can be expressed as

$$|\Psi_{6s+6p}|^2 = |\Psi_{6s}|^2 + |\Psi_{6p}|^2 - \frac{\sqrt{3}}{2\pi}R_{6s}(r)R_{6p}(r)\cos\theta. \qquad (6)$$

Thus, there exists a significant increase (decrease) of the initial electronic density distribution in the $+z$ ($-z$) side, as presented in Fig. 2(g). Furthermore, in the case of $\delta = \pi/2$, the superposition state is $\Psi_{6s+6p} = \Psi_{6p} + i\Psi_{6s}$, thereby the electron probability is given by

$$|\Psi_{6s+6p}|^2 = |\Psi_{6s}|^2 + |\Psi_{6p}|^2. \qquad (7)$$

This indicates that there is no interference between $6s$ and $6p$, and the initial density distribution of the electron is still symmetrical in the $+z$ and $-z$ sides, as shown in Fig. 2(d).

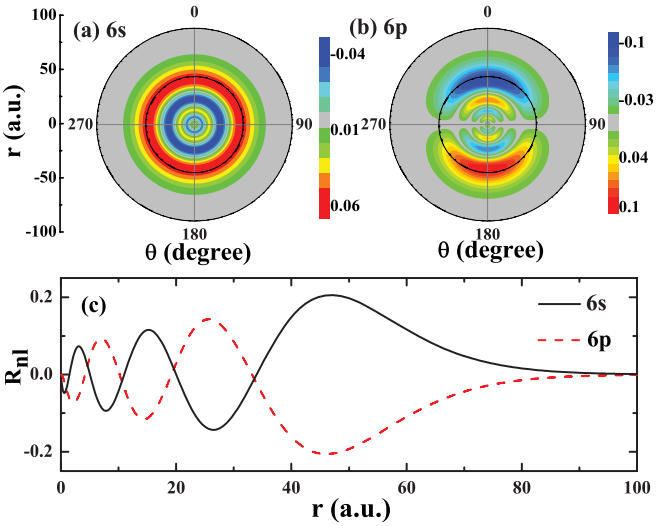

FIG. 1. (Color online) The plots of (a) $6s$ and (b) $6p$ atomic wave functions, and the radial distributions (c) for $6s$ (red dotted curve) and $6p$ (black solid curve).

III. FREQUENCY-SELECTED ENHANCEMENT OF HHG AND ISOLATED ATTOSECOND PULSE GENERATION

We first investigate the evolution process of the superposition state $\Psi_{1s+6s+6p}$ exposed to an infrared laser pulse. The laser's electric field is $E(t) = E_0 \sin^2(\pi t/\tau)\sin(\omega t + \varphi)$, where the laser frequency is $\omega = 0.056$, the carrier envelope phase is $\varphi = 0$, the peak intensity is 3.5×10^{15} W cm^{-2}, and the pulse duration is $\tau = 5.5\,\text{fs} \simeq 2T$, where T is the optical cycle of the driving laser field. Figure 2 shows the electronic density distributions at time $t = 0$ [Figs. 2(a), 2(d), and 2(g)], $0.45T$ [Figs. 2(b), 2(e), and 2(h)], and $0.9T$ [Figs. 2(c), 2(f), and 2(i)] at the relative phase $\delta = 0$ [Figs. 2(a)–2(c)], $\pi/2$ Figs. 2(d)–2(f)], and π Figs. 2(g)–2(i)], respectively. As presented in Fig. 2, although the initial electronic density distributions for the three relative phase cases are different, the dynamic processes of the Rydberg electrons in the laser pulse are consistent. Specifically, the electron first moves toward the $-z$ direction, then is pulled back by the laser field to the core and accelerated toward the $+z$ direction as the laser field changes its direction. On the other hand, the Coulomb focusing

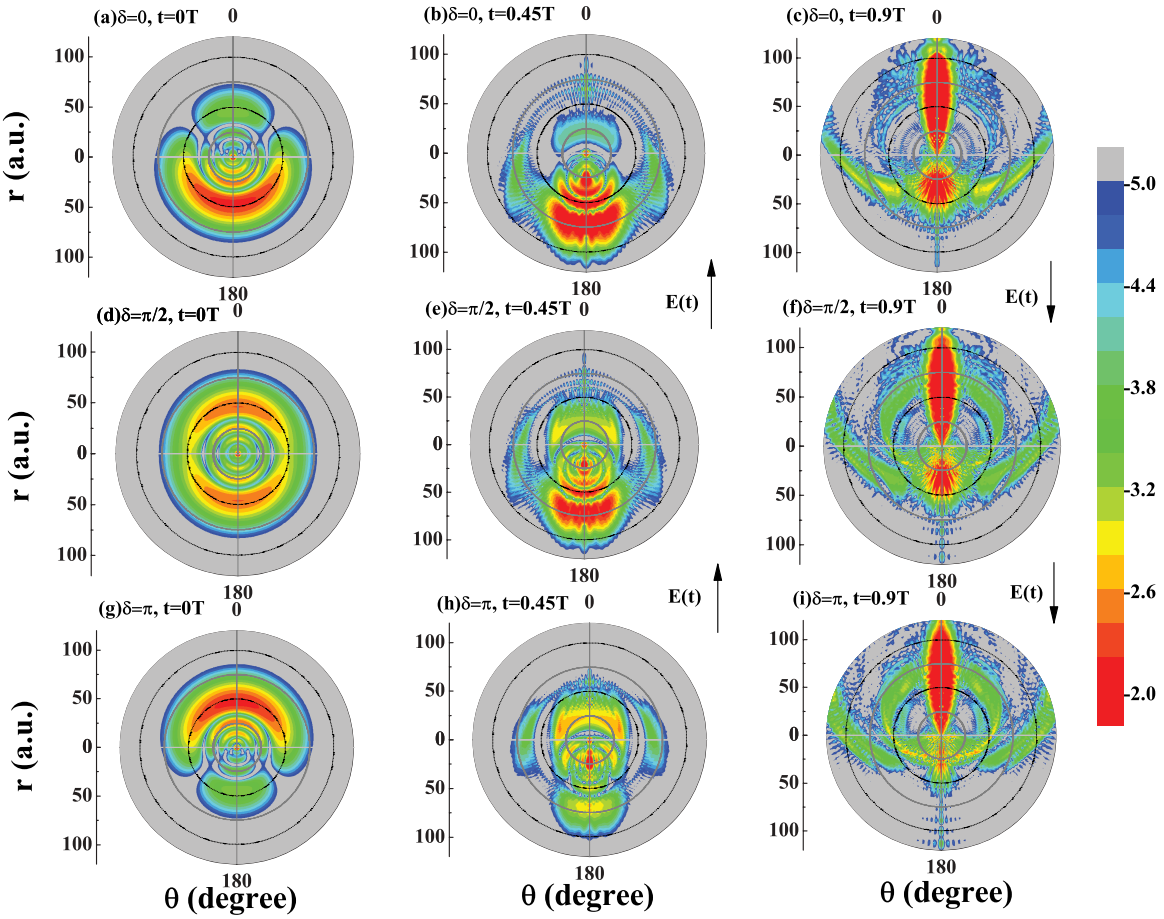

FIG. 2. (Color online) Electronic density distribution of the superposition state $\Psi_{1s+6s+6p}$ with the relative phase (a)–(c) $\delta = 0$, (d)–(f) $\pi/2$, and (g)–(i) π by a 5.5-fs 800-nm laser pulse at the time (a),(d),(g), $t = 0$, (b),(e),(h), $t = 0.45T$, and (c),(f),(i), $t = 0.9T$, where T is the laser cycle. The peak intensity of the pulse is 3.5×10^{15} W cm^{-2}. The directions of the laser electric field are marked by the arrows.

effect on the Rydberg state is weak because of the large radius of the Rydberg state. Therefore, under the interaction of the linearly polarized laser pulse, the largest part of the electronic density undergoes an oscillation and finally is ionized without collision with the core; and only the electron with its density located approximately on the z axis can effectively collide with the core and has a dominant contribution to HHG.

To understand the collision process more clearly between the electron and the core on the z axis, we also study the time evolution of the electronic density distribution along the polarization direction of the driving laser pulse. Figure 3 shows the contour plots of the time-dependent electronic density distributions on the z axis for $\delta = 0$, $\delta = \pi/2$, and $\delta = \pi$. One can observe that the electron initially spreads in the region $|z| \leqslant 70$, and then is oscillated by the driving laser field. For the case of $\delta = 0$, the electron dominates initially on the $-z$ axis, as depicted in Fig. 3(a). Specifically, the electron initially along the $-z$ axis first moves away from the core, then can be accelerated by the laser field toward the core, and collides with the core only once at about $t = 1.0T$. Because of the long acceleration time of the colliding electron, higher-order harmonic can be generated when the electron recombines with the core. On the contrary, for the case of $\delta = \pi$, the electron dominates initially on the $+z$ axis, as presented in Fig. 3(c). In particular, the electron initially located on the $+z$ axis first moves toward the core and then collides with the core twice at about $t = 0.57T$ and $t = 0.75T$ with smaller kinetic energies, which results in the lower-order-harmonic generation. From Figs. 3(a) and 3(c), we find that the initial electronic density along the $-z$ $(+z)$ axis for $\delta = 0$ $(\delta = \pi)$ is apparently enhanced compared with that for $\delta = \pi$ $(\delta = 0)$. Therefore,

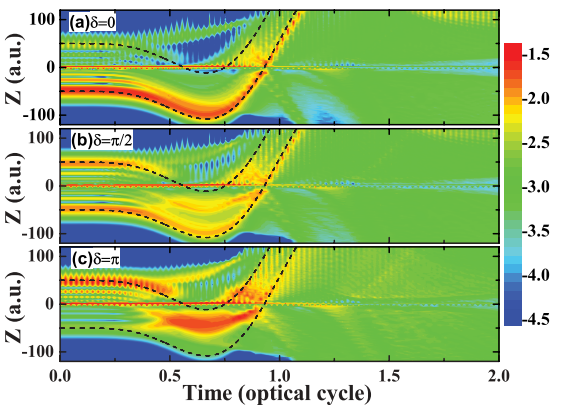

FIG. 3. (Color online) Time evolution of the electronic density distribution on the z axis for the superposition state $\Psi_{1s+6s+6p}$ under different relative phase. The dotted lines are typical classical trajectories.

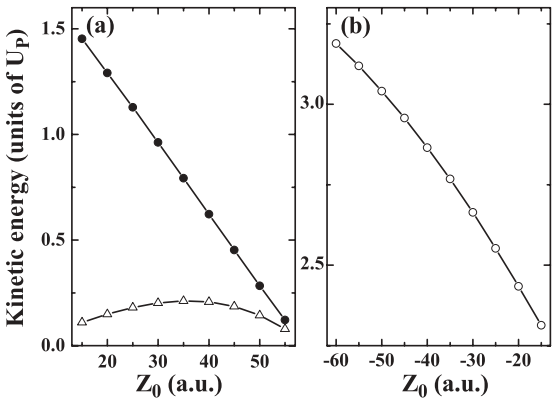

FIG. 4. The kinetic energy of the Rydberg electron at the colliding instant as a function of the initial position Z_0. The open triangle and solid circle lines in (a) show the kinetic energy originating from the first and second collisions, respectively. The laser parameters are the same as those in Fig. 2.

the higher(lower)-order harmonics will be enhanced in the case of $\delta = 0$ ($\delta = \pi$). The above results indicate that the frequency-selected enhancement of HHG may be obtained by changing the initial condition of the Rydberg electron.

The time evolution of the Rydberg electron can also be predicted by the classical trajectories in a combined interaction of Coulomb and laser field, which can be calculated by using a Newtonian equation. The initial position of the electron is set at Z_0 and the initial velocity is taken to be zero due to the small kinetic energy of the Rydberg electron. The dotted lines in Fig. 3 are the typical classical trajectories with $Z_0 = 50$ and $Z_0 = -50$, which agree well with the corresponding evolution of the electronic density distribution by the 3D quantum calculations. In terms of this classical model, we also calculate the kinetic energy of the Rydberg electron at the colliding instant as a function of the initial position. As shown in Fig. 4(a), when the initial position of the electron is located in the region from 15 to 55, because the electron collides with the core twice, there exist two kinetic energies corresponding

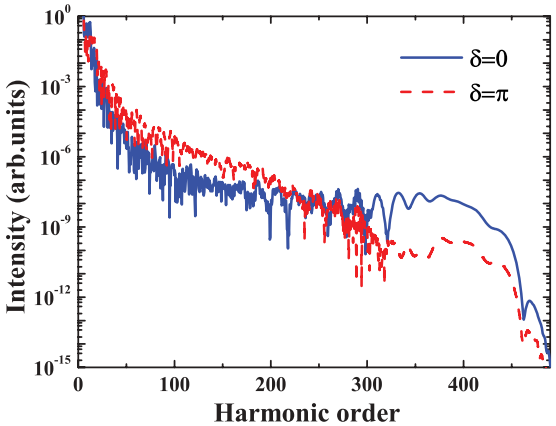

FIG. 5. (Color online) Harmonic spectra from the superposition state $\Psi_{1s+6s+6p}$ by a 5.5-fs 800-nm laser pulse. The relative phase δ between the $6s$ and $6p$ states is set as 0 (blue solid curve) π (red dashed curve), respectively. The laser parameters are the same as those in Fig. 2.

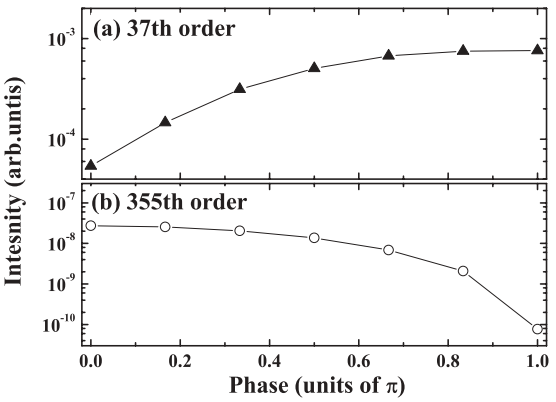

FIG. 6. Dependence of the harmonic intensity on the relative phase δ. The laser parameters are the same as those in Fig. 2.

to the two collisions for each initial position. Specifically, the solid circle line (open triangle line) of the kinetic energy originates from the second (first) collision. The kinetic energy of the solid circle line changes from $0.08U_P$ to $1.45U_P$, which corresponds to the lower-order harmonics from 25th to 220th. On the other hand, when the initial position of the electron changes from -15 to -60, the electron collides with the core only once in the few-cycle laser pulse, and the corresponding kinetic energy changes from $2.13U_P$ to $3.21U_P$, as presented in Fig. 4(b). As a result, we can obtain a broadband continuum harmonic spectrum from 317th to 470th order.

Figure 5 shows the harmonic spectra for the case of $\delta = 0$ (blue solid curve) and $\delta = \pi$ (red dashed curve). It can be seen that, compared to the case of $\delta = \pi$, the intensities of the harmonics near the cutoff region for the case of $\delta = 0$ are increased by more than two orders of magnitude, and the lower-frequency part of the harmonic spectrum is decreased by more than one order of magnitude. This result testifies that the frequency-selected enhancement of HHG can be achieved by controlling the interference of two degenerate Rydberg states in a few-cycle laser pulse. From the above calculations, it can be noticed that the harmonic efficiency is closely related with the relative phase δ between $6s$ and $6p$ Rydberg states. In Fig. 6, taking the 37th (355th) order harmonic as an example, we examine the dependence of the

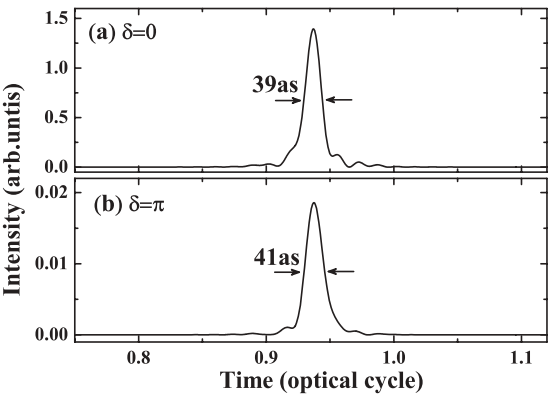

FIG. 7. Temporal profiles of the isolated attosecond pulses by superposing the harmonics from 350th to 420th. The laser parameters are the same as in Fig. 2.

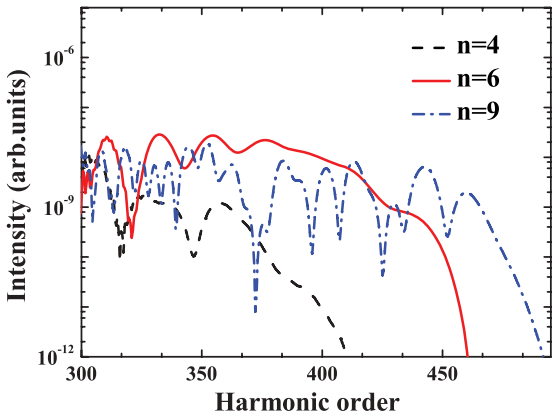

FIG. 8. (Color online) Harmonic spectra from the superposition state $\Psi_{1s+ns+np}$ with $n = 4$ (black dashed curve), 6 (red solid curve), and 9 (blue dot-dashed curve) under the relative phase $\delta = 0$, respectively. The laser parameters are the same as in Fig. 2.

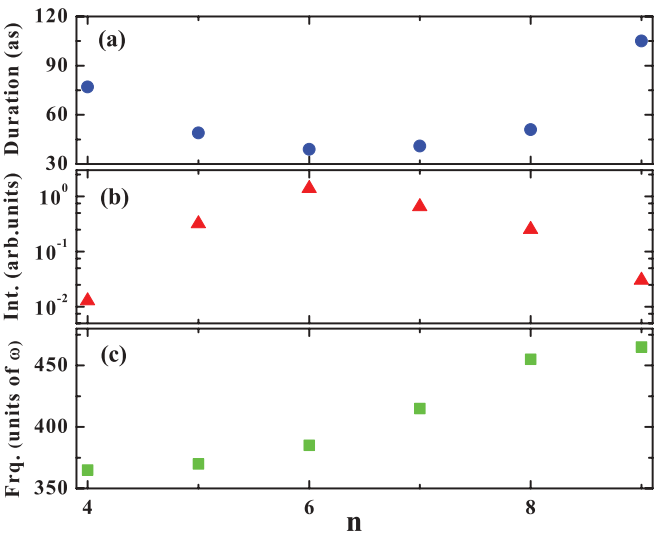

FIG. 9. (Color online) The (a) duration, (b) intensity, and (c) central frequency of attosecond pulse as a function of the principal quantum number, respectively. The attosecond pulse is achieved by superposing the continuum harmonics near the cutoff region.

harmonic intensity on the relative phase δ. One can see that the intensity of the 37th (355th) order harmonic is gradually enhanced (decreased) as the relative phase increases from 0 to π. This arises from the increase (decrease) of the electronic density along the $+z$ ($-z$) axis caused by the interference of $6s$ and $6p$ atomic states. The dependence of the relative phase on the harmonic intensity may open another route to examine the relative phase of degenerate states by HHG.

Taking advantage of the interference of two degenerate states, we can selectively enhance the broadband continuum harmonics near the cutoff of the HHG spectrum. Since only one trajectory contributes to these harmonics, one can expect that an isolated pulse with high intensity can be generated. Figures 7(a) and 7(b) depict the temporal profiles of the attosecond pulses obtained from the continuous spectra corresponding to the blue solid ($\delta = 0$) and red dashed ($\delta = \pi$) curves in Fig. 5, respectively. In the case of $\delta = 0$, an intense isolated 39-attosecond pulse with high signal-to-noise ratio is produced by filtering the harmonics from 350th to 420th order. Moreover, the intensity of the isolated pulse is approximately two orders of magnitude higher than that of the case $\delta = \pi$.

Next, we would like to point out that the selective enhancement of continuum harmonics in different frequency regions can also be realized by changing the peak intensity of the driving laser field and/or adopting a pair of suitable degenerate states, which may lead to intense attosecond pulses with different central frequencies. Figure 8 shows the HHG spectra with $n = 4$ (black dashed curve), 6 (red solid curve), and 9 (blue dot-dashed curve) under the relative phase $\delta = 0$ and the same laser parameters as in Fig. 2. In the present atom-laser condition, our results indicate that the HHG cutoff is increased with the principal quantum number n. By selecting the harmonics in the continuous regions, isolated attosecond pulses can be produced. Figure 9(a) presents the attosecond pulse duration as a function of the principal quantum number n. It is found that an isolated pulse with a duration less than 80 attoseconds can be obtained in the range from $n = 4$ to 8, and the minimum duration of the attosecond pulse is achieved at $n = 6$. Figure 9(b) shows the n dependence of the attosecond pulse intensity, where the maximum value of the intensity also appears at $n = 6$. In our current laser condition, the radial distribution of $n = 6$ can simultaneously ensure the wider bandwidth and the higher intensity of the continuum harmonics [26]. Therefore, $n = 6$ is the optimal quantum number for the generation of an attosecond pulse, as depicted in Figs. 9(a) and 9(b). Figure 9(c) shows that the central frequency of the attosecond pulse is increased with n, which indicates that our method can produce an attosecond pulse in a wide frequency range by altering n. In addition, our simulations also show that one isolated pulse with a duration less than 45 attoseconds can be generated by the driving laser pulse with an intensity ranging from 2.5×10^{15} W cm^{-2} to 5.5×10^{15} W cm^{-2}. The central frequency of the corresponding attosecond pulse changes from 280th to 630th order harmonic.

IV. DISCUSSION AND CONCLUSION

To experimentally realize the asymmetric initial electronic density distribution along the z axis and the frequency-selected enhancement of the continuous HHG, we may apply a combined field of a UV pump laser pulse, a static electric field, and a femtosecond driving laser to interact with the atom [29]. Here, the electric field of the combined field can be expressed as

$$\mathbf{E(t)} = \begin{cases} \hat{z}E_s + \hat{z}E_p \sin^2\left(\frac{\pi t}{\tau_p}\right)\sin(\omega_p t), & 0 \leqslant t \leqslant \tau_p, \\ \hat{z}E_s, & \tau_p \leqslant t \leqslant \tau_p + \tau_d, \\ \hat{z}E_s + \hat{z}E_f \sin^2\left[\frac{\pi(t-\tau_p-\tau_d)}{\tau_f}\right]\sin[\omega_f(t-\tau_p-\tau_d)], & \tau_p + \tau_d \leqslant t \leqslant \tau_p + \tau_d + \tau_f, \end{cases} \quad (8)$$

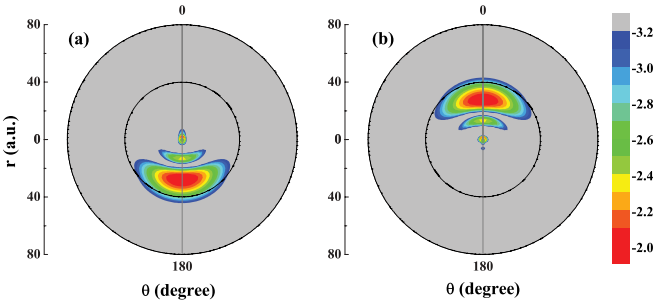

FIG. 10. (Color online) Electronic density distribution for the static electric field along the (a) $+z$ and (b) $-z$ directions. The amplitude of the static electric field is 1.72×10^6 V cm^{-1}, the time delay between the pump laser and the driving pulse is 8.0 fs.

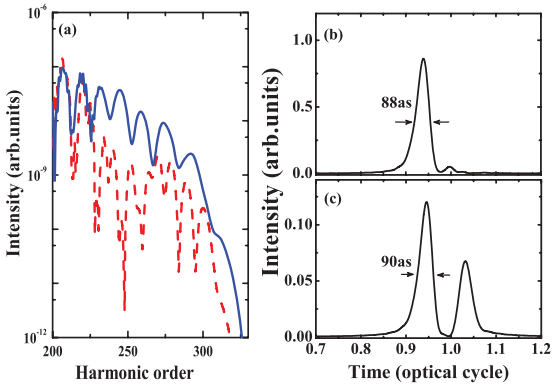

FIG. 11. (Color online) (a) Harmonic spectra for the two prepared initial states evolved by the static field along $+z$ (blue solid curve) and $-z$ (red dashed curve) directions. (b),(c), Temporal profiles of the single attosecond pulses by filtering the harmonics from 280th to 320th in two cases, respectively, are shown. The peak intensity of the few-cycle laser is 2.5×10^{15} W cm^{-2}, the other laser parameters are the same as in Fig. 2.

where E_p, ω_p, and τ_p are the amplitude, frequency, and pulse duration of the UV pump laser, respectively; E_s is the amplitude of the static electric field; E_f, ω_f, and τ_f are the amplitude, frequency, and pulse duration of the femtosecond driving laser, respectively; τ_d is the time delay between the pump laser and the driving pulse.

First, the ground state of the single-active-electron atom model with the ionization potential of neon is excited to a Rydberg state by the pump laser pulse, then this Rydberg state is split by the weak static electric field and forms a superposition of the ground state and the Rydberg states. Here, the pump pulse frequency $\omega_p = 0.77$ a.u., and its intensity is 4.0×10^{13} W cm^{-2} with the pulse duration τ_p being 90 optical cycles; the amplitude E_s of the static electric field is 1.72×10^6 V cm^{-1}. Second, by controlling the time delay τ_d between the pump laser and the driving laser pulse, an asymmetric electronic density distribution along z axis can be realized. Figures 10(a) and 10(b) show the electronic density distribution with the time delay $\tau_d = 8.0$ fs for the static electric field along $+z$ and $-z$ directions, respectively. One can see that the electronic density distribution is very similar as that shown in Figs. 2(a) and 2(g). Finally, the driving laser, which is turned on with a time delay $\tau_d = 8.0$ fs, interacts with the atom with the two initial states presented in Figs. 10(a) and 10(b), the continuum harmonic spectra can be generated, as shown by the solid blue and dashed red curves in Fig. 11(a), respectively. Here, the intensity of the driving laser is 2.5×10^{15} W cm^{-2}. By superposing the harmonics from 280th to 320th in both cases, the isolated pulses with duration 88 and 90 attoseconds can be produced, as presented by Figs. 11(b) and 11(c), respectively. One can see that the intensity of the single pulse in Fig. 11(b) is enhanced approximately one order of magnitude compared to that in Fig. 11(c). This result agrees qualitatively with that shown in Fig. 7. Especially, we should mention that the static electric field is turned on during the entire HHG process. This is possible since the amplitude of the static electric field is much weaker than that of the few-cycle laser pulse, and thus the influence of the static electric field on HHG is of no significance.

In summary, we have proposed a method for the frequency-selected enhancement of HHG by controlling the interference of two degenerate Rydberg states in a few-cycle pulse. The advantage of using degenerate states is that the interference of them can effectively change the initial density distribution of the Rydberg electron, thereby we can control the characteristics and the intensity of HHG. Specifically, our scheme can enhance the broadband continuum harmonics near the cutoff of harmonic spectrum, and an intense isolated pulse with duration less than 100 attoseconds is generated by superposing some properly selected continuous harmonics. Moreover, the intensity of the continuum spectrum is sensitive to the relative phase of the two degenerate Rydberg states, which may open a new way to measure this relative phase by HHG.

ACKNOWLEDGMENTS

This work was supported by NKBRSFC under Grants No. 2011CB921502, No. 2012CB821305, No. 2009CB930701, and No. 2010CB922904; NSFC under Grants No. 10934010, No. 60978019, No. 11074296, and No. 11074026; and NSFC-RGC under Grants No. 11061160490 and No. 1386-N-HKU748/10. JGC acknowledges the support of the Natural Science Foundation of Zhejiang Province under Grant No. Y6110578.

[1] A. McPherson, G. Gibson, H. Jara, V. Johann, T. S. Luk, I. A. McIntyre, K. Boyer, and C. K. Rhodes, J. Opt. Soc. Am. B **4**, 595 (1987).

[2] X. F. Li, A. L'Huillier, M. Ferray, L. A. Lompré, and G. Mainfray, Phys. Rev. A **39**, 5751 (1989).

[3] O. Smirnova, Y. Mairesse, S. Patchkovskii, N. Dudovich, D. Villeneuve, P. Corkum, and M. Yu. Ivanov, Nature (London) **460**, 972 (2009).

[4] M. Lein, N. Hay, R. Velotta, J. P. Marangos, and P. L. Knight, Phys. Rev. Lett. **88**, 183903 (2002).

[5] J. Itatani, J. Levesque, D. Zeidler, H. Niikura, H. Pepin, J. C. Kieffer, P. B. Corkum, and D. M. Villeneuve, Nature (London) **432**, 867 (2004).
[6] T. Kanai, S. Minemoto, and H. Sakai, Nature (London) **435**, 470 (2005).
[7] S. Baker, J. S. Robinson, C. A. Haworth, H. Teng, R. A. Smith, C. C. Chirila, M. Lein, J. W. G. Tisch, and J. P. Marangos, Science **312**, 424 (2006).
[8] R. Torres, N. Kajumba, J. G. Underwood, J. S. Robinson, S. Baker, J. W. G. Tisch, R. de Nalda, W. A. Bryan, R. Velotta, C. Altucci, I. C. E. Turcu, and J. P. Marangos, Phys. Rev. Lett. **98**, 203007 (2007).
[9] B. K. McFarland, J. P. Farrell, P. H. Bucksbaum, and M. Guhr, Science **322**, 1232 (2008).
[10] A. T. Le, R. R. Lucchese, M. T. Lee, and C. D. Lin, Phys. Rev. Lett. **102**, 203001 (2009).
[11] M. Kitzler, X. Xie, S. Roither, A. Scrinzi, and A. Baltuska, New J. Phys. **10**, 025029 (2008).
[12] D. Shafir, Y. Mairesse, D. M. Villeneuve, P. B. Corkum, and N. Dudovich, Nat. Phys. **5**, 412 (2009).
[13] P. B. Corkum, Phys. Rev. lett. **71**, 1994 (1993).
[14] T. Brabec and F. Krausz, Rev. Mod. Phys. **72**, 545 (2000).
[15] G. Winterfeldt, C. Spielmann, and G. Gerber, Rev. Mod. Phys. **80**, 117 (2008).
[16] F. Krausz and M. Ivanov, Rev. Mod. Phys. **81**, 163 (2009).
[17] B. Wang, X. Li, and P. Fu, J. Phys. B **31**, 1961 (1998); Phys. Rev. A **59**, 2894 (1999); **62**, 063816 (2000); P. Fu, B. Wang, X. Li, and L. Gao, *ibid*. **64**, 063401 (2001); B. Wang, T. Cheng, X. Li, P. Fu, S. Chen, and J. Liu, *ibid*. **72**, 063412 (2005).
[18] R. Kienberger, E. Goulielmakis, M. Uiberacker, A. Baltuska, V. Yakovlev, F. Bammer, A. Scrinzi, Th. Westerwalbesloh, U. Kleinberg, U. Heinzmann, M. Drescher, and F. Krausz, Nature (London) **427**, 817 (2004).
[19] G. Sansone, E. Benedetti, F. Calegari, C. Vozzi, L. Avaldi, R. Flammini, L. Poletto, P. Villoresi, C. Altucci, R. Velotta, S. Stagira, S. De Silvestri, and M. Nisoli, Science **314**, 443 (2006).
[20] E. Goulielmakis, M. Schultze, M. Hofstetter, V. S. Yakovlev, J. Gagnon, M. Uiberacker, A. L. Aquila, E. M. Gullikson, D. T. Attwood, R. Kienberger, F. Krausz, and U. Kleineberg, Science **320**, 1614 (2008).
[21] J. G. Chen, Y. J. Yang, S. L. Zeng, and H. Q. Liang, Phys. Rev. A **83**, 023401 (2011).
[22] J. G. Chen, S. L. Zeng, and Y. J. Yang, Phys. Rev. A **82**, 043401 (2010).
[23] R. Bartels, S. Backus, E. Zeek, L. Misoguti, G. Vdovin, I. P. Christov, M. M. Murnane, and H. C. Kapteyn, Nature (London) **406**, 164 (2000).
[24] T. Pfeifer, D. Walter, C. Winterfeldt, C. Spielmann, and G. Gerber, Appl. Phys. B **80**, 277 (2005).
[25] Z. Zhai, J. Chen, Z. C. Yan, P. Fu, and B. Wang, Phys. Rev. A **82**, 043422 (2010).
[26] Z. Zhai, Q. R. Zhu, J. Chen, Z. C. Yan, P. Fu, and B. Wang, Phys. Rev. A **83**, 043409 (2011).
[27] K. C. Kulander, K. J. Schafer, and J. L. Krause, in *Atoms in Intense Laser Fields*, edited by M. Gavrila (Academic, New York, 1992).
[28] B. Wang, J. Chen, J. Liu, Z. C. Yan, and P. Fu, Phys. Rev. A **78**, 023413 (2008).
[29] I. I. Ryabtsev and I. M. Beterov, Phys. Rev. A **61**, 063414 (2000).